

Probing SU(2) Quark Flavor Asymmetry with W Bosons at RHIC

Maximiliano Ponce-Chavez^a

^a*Department of Physics and Astronomy, Michigan State University, East Lansing, 48824, MI, USA*

Abstract

This work examines the effects of multiple parton radiation on proton-proton W^\pm boson production at the Relativistic Heavy Ion Collider (RHIC), focusing on the ratio of charged lepton pseudorapidity differential cross sections to test the SU(2) flavor symmetry violation in the proton quark sea. I show that the measured ratio is minimally affected by the fiducial constraints imposed on the QCD recoil radiation by the STAR experiment, and that the ratio is also stable with respect to transverse momentum resummation effects. Hence, the STAR data on the W^+/W^- cross section ratio provides a robust discrimination of $\bar{d}(x)$ and $\bar{u}(x)$ parton distribution functions (PDFs) at momentum fractions of order 0.1, shown by comparing predictions with various PDF models and using the L_2 sensitivity analysis and reweighting methods.

1. Introduction

Parton distribution functions are fundamental objects that parameterize the internal structure of hadrons in terms of probabilities dependent on the fractional momentum (x) carried by its constituents, namely quarks and gluons, at various resolution energy scales. PDFs are essential for making predictions for hard-scattering experiments involving hadrons, whether to perform tests to the Standard Model or to search for signatures of new physics. Due to their universality (independence from the hard-scattering process [1]), phenomenological parameterizations can be obtained by performing global fits of experimental measurements which are sensitive to PDFs, with the achieved precision depending on both theoretical and experimental inputs, such as the perturbative order of the Quantum Chromodynamics (QCD) elements (scattering amplitudes, splitting functions, etc.), sensitivity of individual experiments to specific PDF flavors [2], and statistical/systematic uncertainties of the experimental data going into the fit. In particular, deep inelastic scattering (DIS) and Drell-Yan pair production experiments are key for separating the proton's valence and sea components, although the latter remains to be well-charted, since the underlying mechanism countering an early parton model assumption of SU(3) flavor symmetry ($\bar{u}(x) = \bar{d}(x) = \bar{s}(x)$) is still under exploration. A summary of past scattering experiments reporting non-negligible deviations from 1/3 in the Gottfried sum rule¹, signaling sea quark flavor asymmetry, is found in Ref. [3]. Dedicated experiments, such as NMC [4, 5], NuSea [6], and SeaQuest [7, 8], measured the ratio of proton-deuteron and proton-proton cross sections, effectively constraining $\bar{d}(x)/\bar{u}(x)$ at moderate and high x , establishing thereupon that the sea-flavor asymmetry is x -dependent. Precise determination of such dependence remains an open question, as measurements from the NuSea and SeaQuest experiments at Fermilab display some tension [7].

Complementing fixed-target measurements, collider-based experiments, *e.g.* the Large Hadron Collider (LHC) [9, 10] and Tevatron [11, 12], place constraints on the proton quark sea through inclusive measurements of lepton charge asymmetry. Furthermore, proton-(anti)proton interactions in collider settings are free from nuclear effects, unlike fixed-target experiments where such effects are assumed to be minimal, but may still impact $\bar{d}(x)/\bar{u}(x)$, pointing to the question of whether the observed asymmetry truly stems from differing contributions in the proton quark sea.

This work focuses on the STAR experiment at BNL's Relativistic Heavy Ion Collider, which explores the flavor asymmetry via the W^\pm cross section ratio of proton-proton scattering at transfer momentum scales significantly

¹Gottfried Sum Rule: $\int_0^1 dx \frac{1}{x} [F_2^p(x) - F_2^n(x)] = \frac{1}{3} + \frac{2}{3} \int_0^1 dx [\bar{u}^p(x) - \bar{d}^p(x)]$. Values different from 1/3 imply $\bar{d}(x) \neq \bar{u}(x)$.

larger than Λ_{QCD} . The STAR collaboration has performed these measurements in sequential runs with unpolarized proton beams; 2011, 2012, 2013 and 2017, with the first three combined in a single dataset [13], while the latest was recently published in Ref. [14]. The ratio of e^\pm pseudorapidity differential cross sections in inclusive production, $pp \rightarrow (W^\pm \rightarrow e^\pm \nu)X$, is sensitive to $\bar{d}(x, Q)/\bar{u}(x, Q)$ at an energy scale of order of the boson’s virtuality $Q \approx M_W \approx 80.4$ GeV. At STAR, W^\pm decay positrons and electrons are registered in the pseudorapidity fiducial region $-1 < \eta < 2$, yielding an approximate fractional momentum coverage of $0.06 < x < 0.4$. The event selection procedure imposes vetoes on charged leptons and jets to reject additional sources of e^\pm production and suppress the large QCD background; these constraints on QCD radiation generally break down the inclusivity of the lepton production process required to apply perturbative QCD factorization. Therefore, the fixed-order $\sigma_{W^+}/\sigma_{W^-}$ ratio calculations in Ref. [13] may be potentially modified by higher-order terms emerging due to the non-inclusive veto on the QCD recoil. This article quantifies the significance of these potential corrections by categorizing radiative contributions arising in the $\sigma_{W^+}/\sigma_{W^-}$ ratio and performing all-order resummation of parton radiation at two perturbative orders.

First, I compare theoretical predictions at the fixed next-to-leading (NLO) and next-to-next-to-leading (NNLO) orders in the strong force coupling (α_s) to those arising from the Collins, Soper and Sterman transverse momentum resummation formalism [15], to evaluate the effects of collinear and soft QCD emissions on the observable e^\pm pseudorapidities. Second, I compare resummed predictions inclusive in QCD recoil to those from the PYTHIA parton showering code [16], in which the STAR-like veto on QCD recoil is imposed, to quantify to what extent the veto leads to deviations. Finally, I compare cross section ratio measurements to analyze the power of STAR data to discriminate among contemporary PDF sets: CT18 [17], MSHT20 [18] and the Hessian versions of NNPDF3.1 [19] and 4.0 [20]. The JAM19 NLO set [21] is also included for fixed-order NLO distributions as a reference for further comparison with future PDF sets published by the JAM collaboration². The resummed differential distributions are computed with the ResBos/ResBos2 [22, 23, 24, 25] code, up to next-to-next-to-next-to-leading logarithm (N³LL) matched to perturbative NNLO. Fixed-order distributions are computed with the MCFM-10.3 code [26, 27, 28].

This paper is organized as follows: Section 2 briefly summarizes the differences between vector boson production with the fixed-perturbative order and resummation prescriptions. Section 3 reviews the differences in the assumptions from STAR’s PYTHIA simulations shaping the experimentally extracted signal and those from the resummed approach. The comparison between experimental data and theoretical predictions with different choices of perturbative orders and PDFs is provided in Section 4. Section 5 details the impact of the new set of measurements mainly on the $\bar{d}(x, Q)$ and $\bar{u}(x, Q)$ distributions of the CT18 PDF set through the L_2 sensitivity study, complemented by a reweighting analysis done on a new PDF set from the CTEQ-TEA collaboration. Additional observations and concluding remarks are presented in Section 6.

2. Fixed-order and resummed computations for inclusive boson production

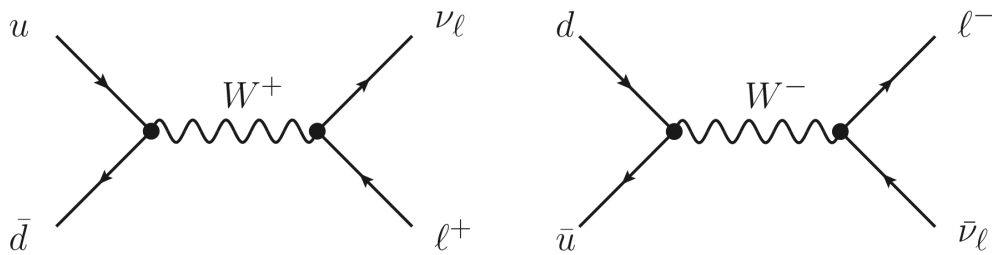


Figure 1: Leading Born-level charged-current vector boson production [29].

The Drell-Yan (DY) process is central to exploring hadronic structure and testing the validity of perturbative QCD, while also being a high-precision probe for measurements of the Standard Model electroweak parameters. The DY

²Internal communication.

hadronic cross section is given by the convolution of a partonic cross section $\hat{\sigma}$, computed as a perturbative expansion in α_s , with PDFs $f_{i/h}(\xi, \mu_F)$ at the characteristic energy scale Q of the partonic process,

$$\sigma_{h_1 h_2 \rightarrow b \nu} = \sum_{i,j=q,\bar{q},g} \int d\xi_1 d\xi_2 [f_{i/h_1}(\xi_1, Q) f_{j/h_2}(\xi_2, Q)] \hat{\sigma}(\xi_1, \xi_2), \quad (1)$$

where the sum runs over all parton flavors within the hadron. In the charged current case at the Born level, up and down-type quarks and antiquarks from various generations annihilate to produce W bosons with null transverse momentum ($q_T = 0$), further decaying into a lepton and the associated neutrino as shown in Fig. 1. Omitting the PDF scale dependence, the proton-proton differential cross section ratio at the Born level in terms of charged boson rapidity y_{W^\pm} is:

$$\frac{d\sigma^{W^+}/dy_{W^+}}{d\sigma^{W^-}/dy_{W^-}} \propto \frac{|V_{ud}|^2 [u(\xi_1)\bar{d}(\xi_2) + \bar{d}(\xi_1)u(\xi_2)] + |V_{us}|^2 [u(\xi_1)\bar{s}(\xi_2) + \bar{s}(\xi_1)u(\xi_2)] + \dots}{|V_{ud}|^2 [\bar{u}(\xi_1)d(\xi_2) + d(\xi_1)\bar{u}(\xi_2)] + |V_{us}|^2 [\bar{u}(\xi_1)s(\xi_2) + s(\xi_1)\bar{u}(\xi_2)] + \dots} \quad (2)$$

$$\approx \frac{u(\xi_1)\bar{d}(\xi_2) + \bar{d}(\xi_1)u(\xi_2)}{\bar{u}(\xi_1)d(\xi_2) + d(\xi_1)\bar{u}(\xi_2)},$$

Leading

with V_{ij} the elements of the Cabibbo-Kobayashi-Maskawa quark flavor mixing matrix, and fractional momenta satisfying $\xi_1 \xi_2 = Q/\sqrt{s}$, where \sqrt{s} is the center-of-mass energy. Within the kinematic coverage of the STAR experiment, Eq. (2) is approximately equal to the leading term in the second line due to the suppression of cross-generation flavor mixing and heavy-quark contributions. In the STAR kinematic region, $u(x, Q)$ and $d(x, Q)$ PDFs are well constrained by DIS data so, in principle, a measurement of the ratio in Eq. (2) would allow the extraction of information about \bar{d}/\bar{u} . However, a direct measurement is not feasible because undetectable neutrinos in the final state impede a unique determination of the W^\pm boson rapidities. Instead, the STAR collaboration measures the cross section ratio as a function of the charged lepton pseudorapidity η_{e^\pm} , which is closely related to the boson rapidity [30]. Moreover, the STAR experiment imposes vetoes on hadronic recoil against the candidate charged leptons, further addressed in Section 3.

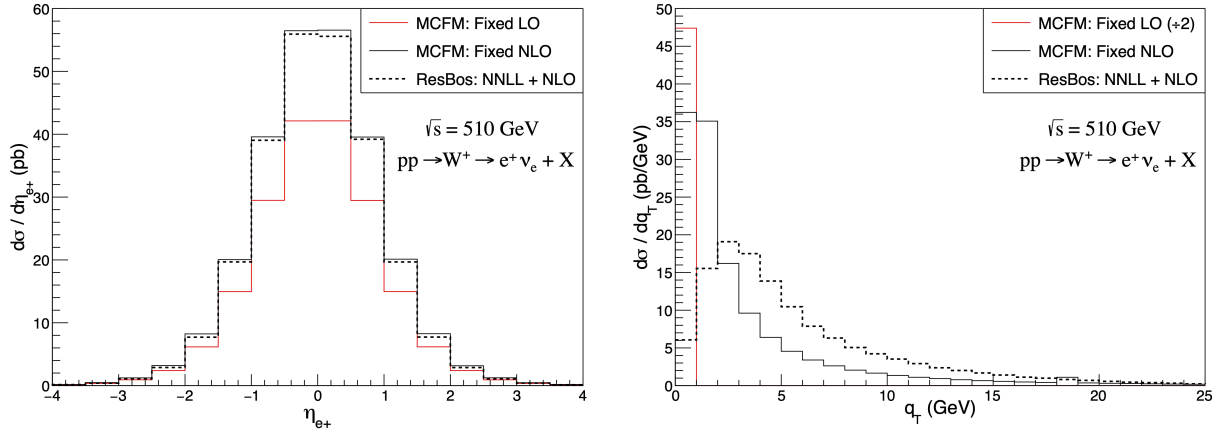


Figure 2: Positron pseudorapidity (left) and vector boson transverse momentum (right) differential cross sections for inclusive W^+ production at $\sqrt{s} = 510$ GeV with fixed-order (MCFM) and resummed (ResBos) calculations at LO and NLO, using the CT18 NNLO PDF set.

Fig. 2 shows lepton pseudorapidity and W boson transverse momentum differential cross sections that are inclusive in QCD radiation, computed up to the fixed NLO, as well as resummed next-to-next-to-leading logarithm matched to NLO. Radiative contributions notably enhance the normalization of the W production rate by a factor $K_{\text{NLO}} \equiv \sigma_{\text{NLO}}/\sigma_{\text{LO}} \approx 1 + \frac{\alpha_s}{2\pi} C_F (1 + \frac{4\pi^2}{3})$ visible in the left panel. As the dominant part of K_{NLO} arises from the hard part of the virtual correction, it is about the same for the fixed-order NLO and resummed cross sections, depending weakly on the rapidity and charge of the boson.

NLO differential cross sections also receive radiative corrections from emission of real gluons and (anti) quarks, creating a spectrum of non-zero boson's transverse momentum q_T , shown in the right panel of Fig. 2. From the perturbative expansion, the transverse momentum differential distribution is logarithmically enhanced at scales much smaller than the characteristic energy ($q_T \ll Q \sim M_W$), with the following behavior:

$$\frac{1}{\sigma} \frac{d\sigma}{dq_T^2} \approx \frac{1}{q_T^2} \left[C_1 \alpha_s \ln \left(\frac{Q^2}{q_T^2} \right) + C_2 \alpha_s^2 \ln^3 \left(\frac{Q^2}{q_T^2} \right) + \dots C_n \alpha_s^n \ln^{2n-1} \left(\frac{Q^2}{q_T^2} \right) \right], \quad (3)$$

where subleading logarithms and (q_T/Q) power corrections are omitted. Consequently, missing higher-order terms contribute to the same extent as any fixed-order truncation, breaking down the convergence of the perturbative expansion. To restore convergence, large logarithms are resummed to all perturbative orders, leading to the Sudakov exponential factor, e^{-S} [15]

$$S(b, Q) = \int_{(b_0/b)^2}^{Q^2} \frac{d\mu^2}{\mu^2} \left[\ln \left(\frac{Q^2}{\mu^2} \right) A(\alpha_s(\mu^2)) + B(\alpha_s(\mu^2)) \right], \quad (4)$$

with μ the resummation energy scale, b the impact parameter, which is the Fourier conjugate of transverse momentum, and $A(\alpha_s)$, $B(\alpha_s)$ are perturbatively calculable coefficients. The Sudakov factor suppresses contributions from large logarithms, resulting in $d\sigma/dq_T \rightarrow 0$ as $q_T \rightarrow 0$ upon inverse Fourier transformation back to q_T space with b -dependent parton distribution functions³. Since the resummed part is only valid at small q_T , to obtain a physical cross section, a component reflecting the convergent perturbative behavior at large q_T and smoothly matched onto the resummed part is required, referred to as the Y function, where the fixed-order expansion of the resummed part is subtracted from the overall fixed-order distribution to remove the singular behavior, giving negligible corrections at small q_T . The right panel of Fig. 2 shows the W^+ transverse momentum differential cross section at fixed-order NLO with the log-enhanced behavior at small q_T , which is suppressed in the NNLL resummed + NLO matched distribution. In contrast, the two distributions have similar convergence for large q_T values. In the subsequent comparisons, we also include resummed contributions from NNLO, contributing a few percent to the total rate and further modifying the q_T dependence. The NNLL+NLO (ResBos [22]) and N³LL+NNLO (ResBos2 [23, 24, 25]) calculations expand A , B and Y functions up to α_s^3 , α_s^2 , α_s and α_s^4 , α_s^3 , α_s^2 orders, respectively. Assessing the robustness of the experimental observable, Fig. 3 shows W^\pm inclusive differential cross sections in e^\pm pseudorapidity at various fixed and resummed orders, with binning and e^\pm fiducial cuts from the STAR experiment, *i.e.* pseudorapidity within the asymmetric detector acceptance volume ($-1 < \eta_e < 1.5$) and transverse energy around the Jacobian peak ($25 \text{ GeV} \leq E_T^e \leq 50 \text{ GeV}$). These predictions are computed with the CT18 NNLO central PDF set [17], setting the factorization and renormalization scales to the dynamical transverse mass $\mu = \sqrt{Q^2 + q_T^2}$. Both the resummed distributions and fixed-order ones are consistent, with minor differences within PDF and scale uncertainty, as expected, since rapidities are mostly sensitive to PDF shapes. NNLO distributions are relatively uniformly enhanced by $\sim 7\%$ compared to the NLO ones.

3. Examination of veto on QCD recoil with PYTHIA

It is important to emphasize that, to be suitable for constraining the PDFs, e^\pm pseudorapidity distributions like the one in the left panel of Fig. 2 and Fig. 3 must be fully inclusive in QCD radiation; this condition is the key assumption behind the provided factorization and resummation formulas. On the other hand, the STAR measurement vetoes hadronic activity inside the fiducial region in order to suppress QCD and electroweak backgrounds, thus breaking the inclusivity condition. Specific acceptance cuts and veto parameters in the STAR analysis can be found in Ref. [14].

To estimate the impact of the veto, the STAR collaboration employs leading-order plus parton shower Monte Carlo (MC) simulations. The impact of a veto is reviewed here, using one of the STAR simulations [32] with the PYTHIA parton shower [16]. Comparing these predictions to the inclusive resummed ones poses a challenge at various levels, as the treatment of QCD radiation is not equal in the two approaches. First, NLO virtual corrections are not present in

³Details of the resummation formalism for W boson production at RHIC can be found in [30, 31] and for CSS resummation in [15, 29, 22, 23].

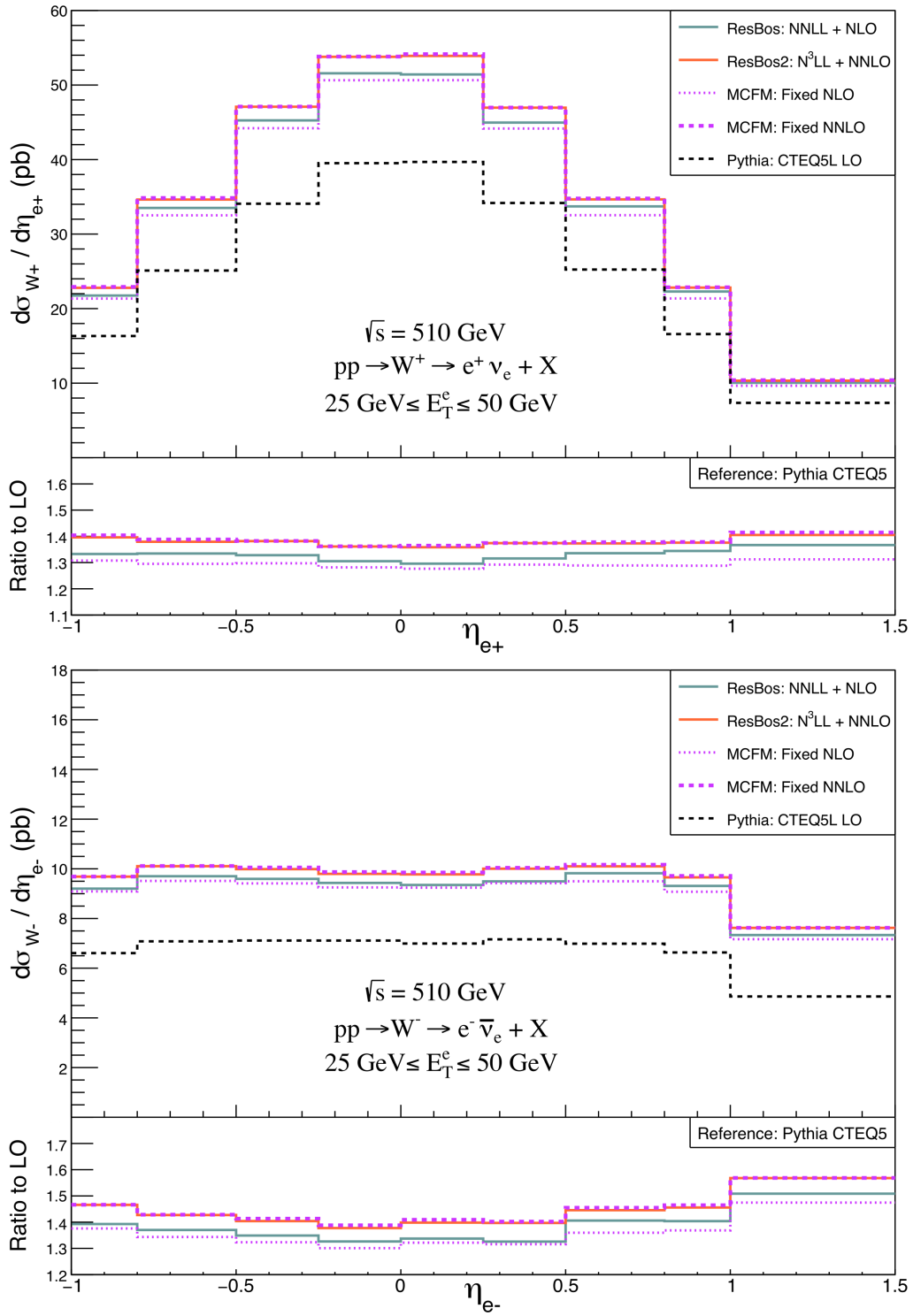


Figure 3: Predicted lepton pseudorapidity differential cross sections (pb) for W^+ (upper) and W^- (lower) boson production with lepton cuts at $\sqrt{s} = 510$ GeV. Theoretical predictions are QCD-inclusive, *i.e.* no cuts are imposed in the phase space of radiated gluons. $\mathcal{O}(\alpha_s^2)$ and $\mathcal{O}(\alpha_s)$ distributions differ in normalization by $\sim 7\%$.

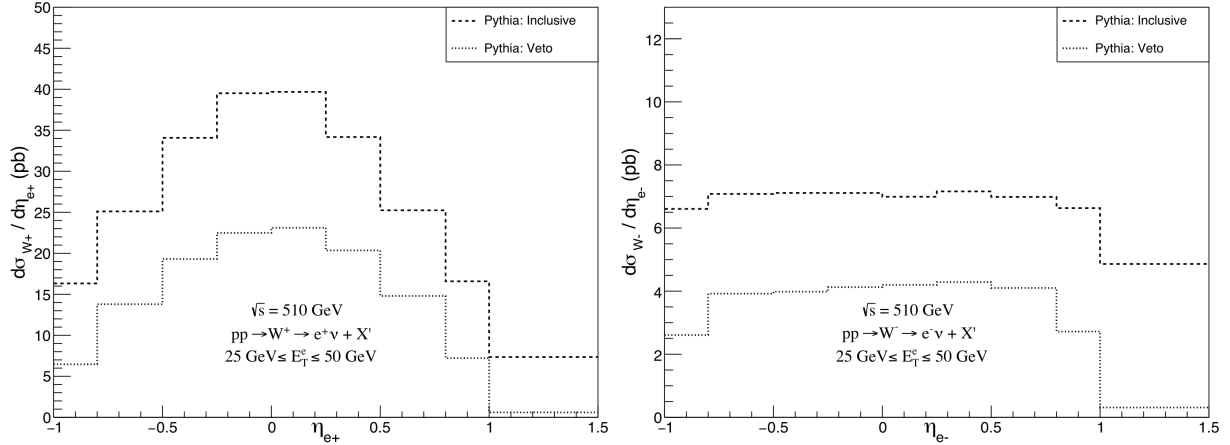


Figure 4: Pythia LO lepton pseudorapidity cross sections (pb) for W^+ (left) and W^- (right) cross sections at $\sqrt{s} = 510$ GeV and using CTEQ5L PDFs, with and without vetoes on QCD radiation.

PYTHIA, i.e. the kinematically independent factor $K_{\text{NLO}} \sim (1 + 3.005\alpha_s) \approx 1.36$ is missing both in the PYTHIA total rate and differential distributions. Thus, the inclusive LO PYTHIA predictions shown in Fig. 3 are 30-40% lower than the NLO ones. The impact of the missing virtual correction on the distribution shape is weak in the pseudorapidity range corresponding to the barrel calorimeter ($|\eta_e| < 1$), as seen in the subpanels of Fig. 3, where the ratio of higher-order distributions to PYTHIA LO is taken. Note that the (N)NLO/PYTHIA ratio is slightly larger for W^- in the STAR endcap calorimeter [33] pseudorapidity bin ($1 < \eta_e < 1.5$), possibly induced by the PDF choice in the PYTHIA simulation, since the STAR collaboration generates PYTHIA simulations with the leading-order CTEQ5L set [34], which behaves substantially differently from the modern CT18 (N)NLO PDF sets. Second, a correction from the parton to detector level in PYTHIA independently reduces both W^\pm cross sections by an additional factor of $\sim 40\%$, shown in Fig. 4. This behavior is approximately uniform, suggesting that the effects of the STAR experimental assumptions generally cancel out in the STAR barrel calorimeter region ($|\eta_e| < 1$) [35] once the e^\pm pseudorapidity differential cross section ratio is obtained, as discussed in Section 4. In contrast, the differential cross section in the pseudorapidity bin ($1 < \eta_e < 1.5$) corresponding to the endcap calorimeter [33] is severely reduced by the vetoes.

4. Comparison to STAR measurements of W^+/W^- cross section ratios

The left panel of Fig. 5 shows the differential cross section ratio, $R_{+/-} \equiv (d\sigma_{W^+}/d\eta_{e^+})/(d\sigma_{W^-}/d\eta_{e^-})$, computed at the QCD-inclusive fixed-order LO and resummed NLO and NNLO with the CT18 NNLO PDF set. It is evident that the differences due to normalization and resummation in the W^\pm cross sections from Fig. 3 largely cancel out in the QCD-inclusive cross section ratio. Comparing it at different orders and setting the N³LL+NNLO distribution as the baseline, the lower subpanel of Fig. 5 shows variations of at most $\sim 2\%$ across all pseudorapidity bins for distributions with the same PDF set, supporting the argument that this observable is robust with respect to perturbative corrections [14], while being informative about flavor asymmetry in the proton quark sea. The right panel of Fig. 5 shows the cross section ratio from the PYTHIA simulations; the distributions with and without the hadronic veto are generally consistent, except at the bin of highest pseudorapidity where the effects of vetoes are substantial, noting that this region maps to the fractional momentum region where $\bar{d}(x)/\bar{u}(x)$ is in tension for deuteron scattering experiments. The inclusive N³LL+NNLO prediction has a similar overall agreement with the veto distribution in the barrel calorimeter region, as shown in the lower subpanel where the ratio to the resummed distribution is taken. Deviations between the ResBos2 and PYTHIA distributions also arise from the choice of a different PDF set, CTEQ5L [34]. Additionally, the ratio of PYTHIA distributions was obtained to estimate the scaling factors from vetoed to inclusive level. These scaling factors are employed in the PDF reweighting analysis in Section 5.

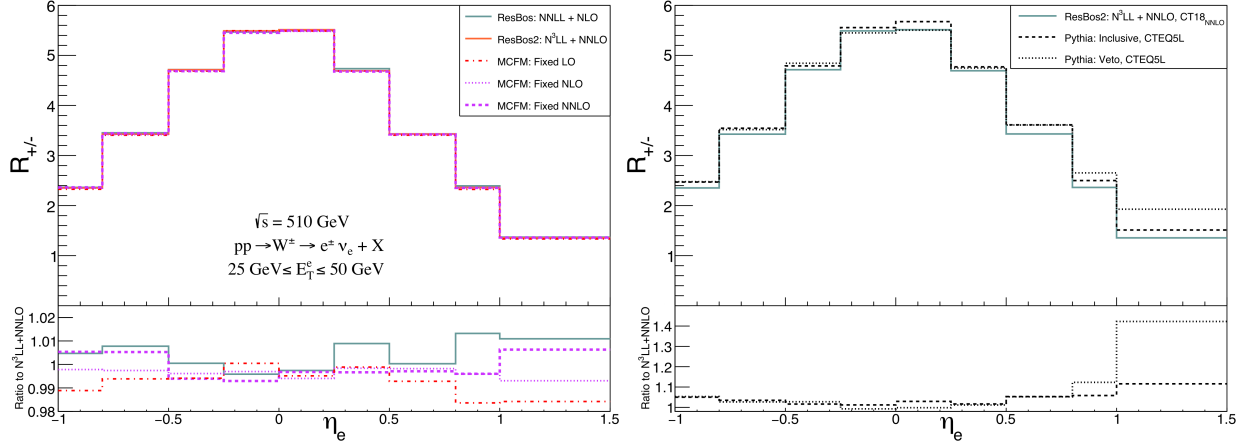


Figure 5: Predictions for QCD-inclusive lepton pseudorapidity differential cross section ratio with various perturbative prescriptions for W^\pm production at $\sqrt{s} = 510$ GeV.

Pseudorapidity Bin	$ \eta_e < 0.25$	$0.25 < \eta_e < 0.5$	$0.5 < \eta_e < 0.8$	$0.8 < \eta_e < 1.0$	$1.0 < \eta_e < 1.5$
Scaling Factor	1.03	0.997	1.00	0.970	0.784

Table 1: Scaling factors to correct STAR data from veto to inclusive level, obtained from the ratio of PYTHIA inclusive to PYTHIA veto $R_{+/-}$ distributions, averaging over symmetric lepton pseudorapidity bins.

Next, Fig. 6 examines the PDF variation of $R_{+/-}$, assuming that the perturbative prescription has negligible effects on the distribution. For ResBos2 $N^3LL+NNLO$ predictions, the CT18, MSHT20, NNPDF3.1 and NNPDF4.0 sets are considered, and JAM19 for fixed NLO with MCFM-10.3. Select PDF uncertainty bands are computed at 68 % confidence level for sets with different parameterization frameworks; CT18 for Hessian/polynomial, NNPDF4.0 for MC/neural network, and JAM19 for MC/polynomial. NNLO predictions are clustered in a central region covered by the CT18 band, showing general agreement between the global fitting groups, whereas JAM19's central ratio and uncertainty band lie outside this region, caused by higher and lower W^\pm cross sections, respectively, preventing this set from reconstructing STAR's $R_{+/-}$ data points. It is important to note that the JAM19 analysis simultaneously determines unpolarized proton PDFs and parton fragmentation functions, fitting to data differently from the NNLO sets [21, 36].

Set	CT18	MSHT20	NNPDF3.1	NNPDF4.0	JAM19
χ^2/N_{pt} , Combined Pre-'13	3.36 (2.88)	3.24 (2.77)	3.06 (2.63)	4.26 (3.77)	24.7 (24.1)
χ^2/N_{pt} , '17 (Preliminary)	1.17 (1.08)	1.10 (1.01)	1.17 (1.15)	1.44 (1.39)	19.3 (19.6)
χ^2/N_{pt} , All-Years Average	3.54 (2.88)	3.35 (2.70)	3.53 (2.96)	5.21 (4.53)	44.0 (43.2)

Table 2: Reduced χ^2 for central predictions of various PDF sets to differential cross section ratio measurements from the STAR experiment with and without veto to inclusive correction factors. Since the bin of highest pseudorapidity is discarded for rescaling, its correction factor is arbitrarily set to 1 here. Accounting for correction in this bin significantly increases χ^2 for NNLO sets.

Table 2 reports the reduced χ^2 measure, assessing the agreement of central PDF predictions of $R_{+/-}$ with STAR's measurements from the preceding ('11+'12+'13, further referred to as *combined pre-'13*) and latest ('17) datasets, as published (in parenthesis) as well as after correcting the data to the inclusive level (approximately) by scaling with factors from Table 1, discarding the highest pseudorapidity bin due to the large differences with inclusive distributions. Note that the '17 dataset still shows a good agreement with the central NNLO PDF predictions after correction.

Consistently with an observation in Ref. [13], this study reports that the combined pre-'13 experimental points and inclusive theoretical distributions broadly follow the same trend. For this dataset, the χ^2 is enhanced mainly due

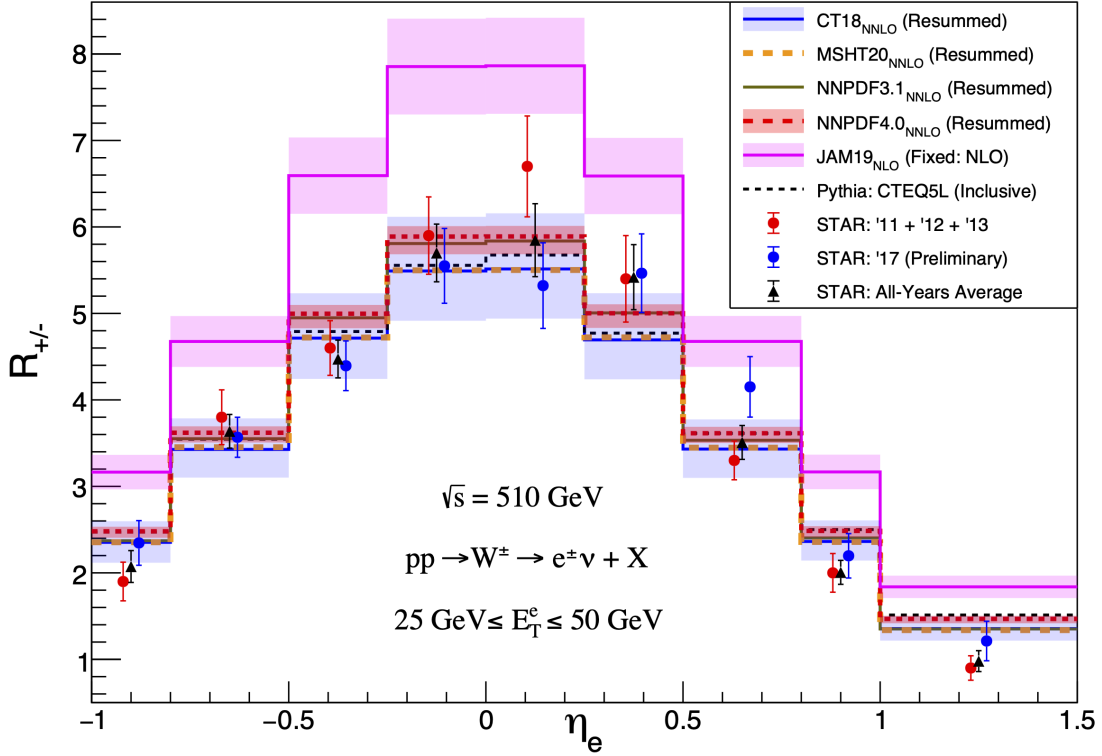


Figure 6: Experimental and resummed $\sigma_{W^+}/\sigma_{W^-}$ cross section ratios for various PDF sets. Uncertainty bands are given at 68% confidence level. Systematic and statistical uncertainties are combined in quadrature for all data points, and the veto to inclusive correction is not applied.

to the first, fifth, eighth, and ninth pseudorapidity bins, where the overlap between experimental error bars and central predictions with and without PDF uncertainties is marginal or null. Consequently, the reduced χ^2 values in the first row of Table 2 differ significantly from unity. In contrast, the '17 preliminary dataset yields significant improvements in χ^2 , as data points previously showing poor agreement generally lie near the cluster of central NNLO predictions, including the bin of highest pseudorapidity, where the theory-data overlap is now within uncertainty, thus shifting the reduced χ^2 closer to unity. Finally, the average of all STAR datasets generally remains close to the NNLO predictions in most bins, however, χ^2 does not reduce due to decrements in experimental error bars caused by higher statistics, particularly for the two last data points.

5. Estimated impact of STAR data on PDFs

To evaluate the effect on sea-quark distributions prior to the inclusion of the latest STAR cross section ratio measurements in a PDF fit, sensitivity and reweighting analyses were performed on PDF sets published by the CTEQ-TEA group. First, following the studies in Refs. [2, 37, 38], the statistical pull induced on PDFs by the data-theory residuals is analyzed through the L_2 sensitivity:

$$S_{f,L_2}^H(x, Q) = \delta_H(\chi^2) C_H(f(x, Q), \chi^2), \quad (5)$$

where $\delta_H(\chi^2)$ is the Hessian symmetric uncertainty of STAR's total χ^2 and $C_H(f(x, Q), \chi^2)$ is the Pearson correlation cosine between a PDF $f(x, Q)$ and χ^2 . From Ref. [39], for a variable X depending on a PDF fitted with D parameters,

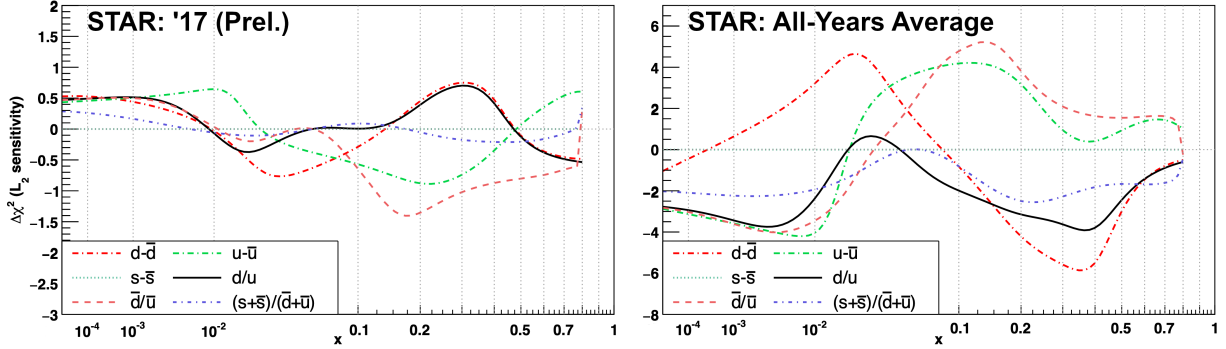


Figure 7: CT18 NNLO sensitivity plots for PDF flavor combinations at $Q = 2$ GeV, 68% confidence level, with STAR's '17 preliminary (left) and all-years average (right) residuals.

the Hessian uncertainty at the confidence level determined by the PDF set is defined as:

$$\delta_H(X) = \frac{1}{2} \sqrt{\sum_{i=1}^D [X_{+i} - X_{-i}]^2}, \quad (6)$$

with $X_{\pm i}$ denoting the variable evaluated with the i -th positive/negative eigenvector error PDF, while the correlation cosine is given by:

$$C_H(f(x, Q), \chi^2) = \frac{1}{4\delta_H(f(x, Q)) \delta_H(\chi^2)} \sum_{i=1}^D [f_{+i}(x, Q) - f_{-i}(x, Q)] [\chi_{+i}^2 - \chi_{-i}^2]. \quad (7)$$

Therefore, $S_{f, L_2}^H(x, Q)$ estimates the change in χ^2 when the PDF increases by one error unit, at given x and Q values, with negative sensitivity values implying an anticorrelation between χ^2 and PDF increments, consequently pulling $f(x, Q)$ upward to better match the experimental observable. Conversely, positive sensitivities indicate downward pulls on $f(x, Q)$. For this analysis, the CT18 central set and its 58 error eigenvectors ($D = 29$ in Eqs. 6,7) are chosen. The residuals are computed by comparing the $R_{+/-}$ '17 preliminary and all-years averaged experimental measurements with the NNLL+NLO predictions from all CT18 error sets. The L_2 sensitivity to residuals with the '17 dataset is shown in the left panel of Fig. 7 for indicated combinations of CT18 NNLO PDFs at $Q = 2$ GeV. Specifically, $\bar{d}(x)/\bar{u}(x)$ shows a negative sensitivity, with the reduction of χ^2 peaking near $x \sim 0.2$, precisely covered by the detector fiducial volume and indicating that the STAR '17 measurements prefer a slightly enhanced ratio in the large- x region. Examination of the sensitivities of individual PDF flavors reveals that this pull is primarily induced by a reduction in $\bar{u}(x)$, associated with a positive value of the corresponding sensitivity⁴. In contrast, the combined dataset (right panel) drastically generates the opposite effect with stronger downward χ^2 pulls on the \bar{d}/\bar{u} ratio induced by a significant increase of $\bar{u}(x)$ at $x \sim 0.1$.

The most recent global QCD analysis by the CTEQ-TEA collaboration produced CT25 [40, 41], a NNLO PDF set with newly incorporated LHC data and alternative prescriptions to account for epistemic uncertainty, *i.e.* pertaining to PDF parameterizations and fitting methodology. Among those, the CT25 flat prior NNLO PDF set (further referred to as *CT25FlatP*) is of particular interest for this work. CT25FlatP, fully described in the upcoming journal publication [41], is made up of $N = 350$ PDF central solutions describing the proton-only subset from the global fit's data pool *as good* as the nominal CT25 NNLO set. The distinguishing feature of CT25FlatP is that all of its sets are fits with good χ^2 for the proton-only subset of the CT25 baseline, obtained either by statistical fluctuations of the data points or by changes in the PDF parametrizations. The distribution of the CT25FlatP sets can thus be taken as a prior that can be

⁴Sensitivity plots for individual PDF flavors are omitted for brevity.

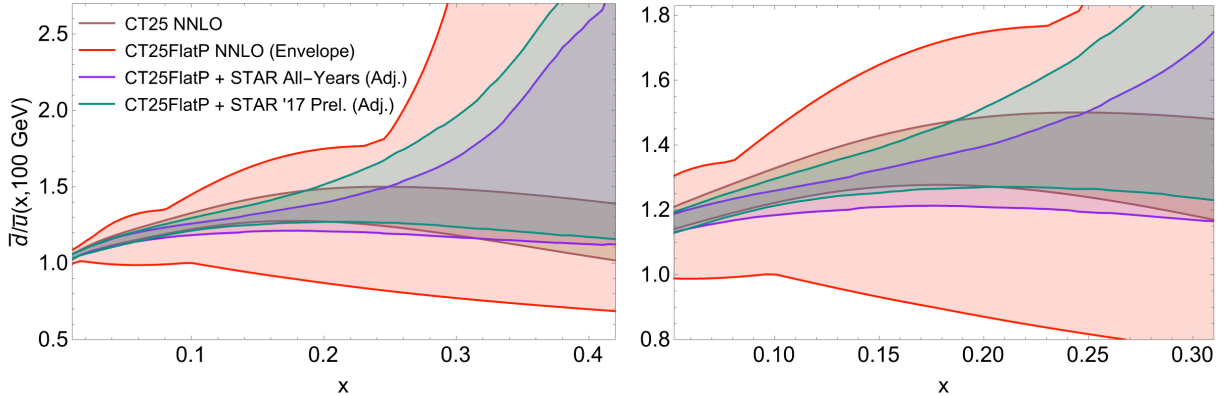


Figure 8: $\bar{d}(x)/\bar{u}(x)$ uncertainty bands at $Q = 100$ GeV for the CT25 NNLO and CT25FlatP sets. Reweighted bands are computed asymmetrically with adjusted weights from Eq. (10). The right figure is an amplification of the left figure into the highest sensitivity fractional momentum region from the STAR experiment.

updated by the STAR measurements, offering yet more constraints to the proton sea-quark PDFs with the advantage of being free of potential bias from nuclear effects. Before reweighting, the density of the CT25FlatP predictions does not carry probabilistic meaning, as all 350 input sets are equally acceptable in this approach. The CT25FlatP prior uncertainty therefore is given by an envelope of all predictions. After the reweighting, the posterior probability of a CT25FlatP member set is given by a weight dependent on the χ^2 of the STAR measurement, with the explicit formulas given at the end of this section.

Motivated by the constraining power of the STAR measurements, Fig. 8 shows the CT25FlatP uncertainty for $\bar{d}(x, Q)/\bar{u}(x, Q)$ at $Q = 100$ GeV before and after reweighting by the $R_{+/-}$ ratio from the '17 preliminary and all-years averaged datasets. The STAR data is corrected to the QCD-inclusive level using the factors in Table 1, recalling that the highest pseudorapidity bin ($1 < \eta_e < 1.5$) is excluded from this analysis due to the large difference between the vetoed and inclusive $R_{+/-}$ predictions, as well as its large χ^2 . The error bands from the nominal CT25 NNLO at 68% confidence level (in brown) and the “flat prior” CT25FlatP (in red) ensembles are compared first. In the former, the $\bar{d}(x)/\bar{u}(x)$ ratio is constrained at $x > 0.1$ by a combination of $\sigma_{pd}/2\sigma_{pp}$ measurements by the NuSea [6] and SeaQuest [7, 8] fixed-target Drell-Yan experiments. This constraint is not imposed on the CT25FlatP set, so the $\bar{d}(x)/\bar{u}(x)$ uncertainty of this set is much wider than the CT25 one. Large variations in this region are reflected by the envelope of CT25FlatP solutions, realized for some parameterizations.

Fig. 8 also shows standard deviations on $\bar{d}(x)/\bar{u}(x)$ obtained by reweighting with the '17 preliminary and all-years averaged STAR datasets (green and violet, respectively), with weights corresponding to the $\Delta\chi^2 = 1$ tolerance criterion for the PDF uncertainty, suitable when the experiment dominates without tension with other experiments, and given that the CT25FlatP prior already accounts for the PDF parametrization uncertainty.⁵ The reweighted PDFs are consistent with CT25 NNLO, although the all-years averaged dataset, with its elevated overall χ^2 for CT18 NNLO in Table 2, prefers a lower $\bar{d}(x)/\bar{u}(x)$ in the most sensitive x region. Overall, the STAR measurement is compatible with $\bar{d}/\bar{u} \approx 1.25$ at $x \approx 0.15$ already expected based on the NuSea/SeaQuest observations. It is substantially incompatible with $\bar{d}(x)/\bar{u}(x)$ equal to one or less than one, values that might be allowed in other analyses [42, 43].

For each reweighted $\bar{d}(x, Q)/\bar{u}(x, Q)$, denoted by f , the central (expectation) value f_* is given by the weighted average over $N = 350$ CT25FlatP member sets:

$$f_* \equiv \frac{1}{\sum_{k=1}^N w_k} \sum_{k=1}^N w_k f_k. \quad (8)$$

⁵This uncertainty may be increased in the full global analysis if there are tensions with other experiments.

The reweighted positive and negative uncertainties are asymmetric weighted standard deviations with Bessel correction, computed by

$$\begin{aligned}\delta^+ f &= + \sqrt{\frac{\sum_{f_k > f_*} w_k}{\left(\sum_{f_k > f_*} w_k\right)^2 - \sum_{f_k > f_*} w_k^2} \cdot \sum_{f_k > f_*} w_k \cdot (f_k - f_*)^2}, \\ \delta^- f &= - \sqrt{\frac{\sum_{f_k < f_*} w_k}{\left(\sum_{f_k < f_*} w_k\right)^2 - \sum_{f_k < f_*} w_k^2} \cdot \sum_{f_k < f_*} w_k \cdot (f_* - f_k)^2}.\end{aligned}\tag{9}$$

The factors w_k are generalized Giele-Keller weights,

$$w_k \equiv \frac{a_k e^{-\frac{1}{2}\chi_k^2}}{\frac{1}{N} \sum_{k=1}^N a_k e^{-\frac{1}{2}\chi_k^2}}.\tag{10}$$

Here, χ_k^2 is constructed from STAR central values and uncertainties for $R_{+/-}$ corrected to the QCD-inclusive level, not including the highest η_e bin, as well as from the NNLL+NLO prediction for $R_{+/-}$ based on the k -th CT25FlatP member set. The choice $a_k = 1$ corresponds to the original Giele-Keller (GK) weight [44], introduced to update probabilities of discrete member sets outside of full refitting:

$$\text{Giele-Keller: } w_k^{\text{GK}} = \frac{e^{-\frac{1}{2}\chi_k^2}}{\frac{1}{N} \sum_{k=1}^N e^{-\frac{1}{2}\chi_k^2}}.\tag{11}$$

Non-unit factors $a_k \neq 1$ are allowed to account for the variable density of sampling of $f = \bar{d}/\bar{u}$ by CT25FlatP predictions. Here, f refers to $\bar{d}(x)/\bar{u}(x)$ at $x = 0.15$ and $Q = 100$ GeV. The important point to notice is that the density of sampling of f_k values with CT25FlatP member sets is distinct from the sets' probabilities based on their agreement with the prior data (proton-only baseline). All CT25FlatP members approximately have the same prior probability, given their nearly equal χ^2 for the proton-only baseline, regardless of where f_k falls in the full span $f_{\min} \leq f \leq f_{\max}$ of the CT25FlatP envelope.

Regarding the distribution of f_k at $x \approx 0.15$, corresponding to rapidity $y \approx 0$ for the STAR kinematics, the middle of the envelope ([1.2–1.4]) is densely sampled due to the way the CT25FlatP PDFs are constructed, in particular, because a large number of member sets originate from fits including deuteron data. On the other hand, the less common members at the edges of the span (*e.g.*, obtained with distinct PDF parametrizations that are allowed in the absence of the deuteron constraints) are as good as the ones in the middle region. Accounting for the density of member sets, the weights in Eq. (10) can be adjusted by setting the a_k factors to be inversely proportional to the CT25FlatP f_k prior density found by a kernel density estimation⁶. For the observed f_k distribution, the a_k factors increase w_k for member sets at the tails, while lowering the weights within the central [1.2, 1.4] interval. The CT25FlatP PDFs were reweighted using the adjusted and the original Giele-Keller weights in Eqs. (10) and (11), finding the differences between these prescriptions to be minimal. Only the prescription of adjusted weights is presented in Fig. 8, with the reweighted bands based on the original Giele-Keller weights being close to the shown ones.

6. Conclusions

In this work, I have explored the impact of hadronic vetoes on W^\pm boson production e^\pm pseudorapidity differential cross sections at RHIC, focusing on their ratio, which is sensitive to the sea-quark flavor asymmetry in the proton. Comparing fixed-order and resummed inclusive predictions with leading-order parton showering simulations, I observed that differences arising from normalization and the hadronic recoil veto mostly cancel out in the cross section ratio for pseudorapidities within the STAR barrel calorimeter volume, although notable deviations induced by the veto

⁶The a_k factors can be alternatively estimated by histogramming the f_k values and taking the inverses of the counts in each f_k bin.

remain in the endcap calorimeter region, with Table 1 listing the approximate factors to correct the $\sigma_{W^+}/\sigma_{W^-}$ ratios from the vetoed to QCD-inclusive level. Then, the preliminary dataset of STAR’s pseudorapidity ratio measurements in 2017 was compared with inclusive resummed central predictions using various modern PDF sets, showing notable reductions in χ^2 in contrast to the STAR measurements from the earlier years. Both a L_2 sensitivity analysis done with the CT18 NNLO PDF set and reweighting of the CT25 Flat Prior set indicate that the STAR result agrees with $\bar{d}(x, Q)/\bar{u}(x, Q) \approx 1.25$ at $x = 0.15$ and $Q = 100$ GeV. Reweighting the CT25FlatP *proton-only* set with the STAR data significantly reduces the uncertainty on $\bar{d}(x)/\bar{u}(x)$, see Fig. 8. The reweighted $\bar{d}(x)/\bar{u}(x)$ ratio at $x \approx 0.15$ is slightly lower, specially for the combined STAR dataset from all years, than the nominal CT25 one which includes the Nusea/SeaQuest $\sigma_{pd}/(2\sigma_{pp})$ Drell-Yan data, but remains in agreement with CT25 within the reweighted PDF uncertainty while being inconsistent with the SU(2)-symmetric $\bar{d}/\bar{u} = 1$. Therefore, this work shows that the $\sigma_{W^+}/\sigma_{W^-}$ cross section ratio measurements by the STAR collaboration can constrain the light sea-quark distributions in the proton with the advantage of being free of nuclear effects. The main findings presented here are based on the preliminary 2017 STAR measurements and on the application of PDF sensitivity and reweighting techniques to published PDF sets. A more complete assessment will be obtained after the publication of the final STAR results by including them into the CTEQ-TEA global fit, together with other sensitive fixed-target deuteron and LHC measurements.

7. Acknowledgments

I would like to thank Pavel Nadolsky and colleagues at Michigan State University for insightful discussions and detailed instruction on the usage of the resummation codes. Also, I want to thank Jae D. Nam for the close communication regarding the STAR experiment, and Aurore Courtoy as well as her research group for fruitful interactions at IFUNAM. This work was supported by the U.S. National Science Foundation under Grant No. PHY-2310291; by the Wu-Ki Tung Endowment and partially by the UNAM Grant No. DGAPA-PAPIIT IN102225.

References

- [1] CTEQ Collaboration, R. Brock *et al.*, “Handbook of perturbative QCD: Version 1.0” *Rev. Mod. Phys.* **67** (1995) 157–248.
- [2] X. Jing *et al.*, “Quantifying the interplay of experimental constraints in analyses of parton distributions,” *Phys. Rev. D* **108** no. 3, (2023) 034029, [arXiv:2306.03918 \[hep-ph\]](#).
- [3] J.-C. Peng and G. T. Garvey, “Flavor asymmetry of the sea quark distributions,” [arXiv:hep-ph/9912370](#).
- [4] New Muon Collaboration, P. Amaudruz *et al.*, “The Gottfried sum from the ratio $F_2(n)/F_2(p)$,” *Phys. Rev. Lett.* **66** (1991) 2712–2715.
- [5] New Muon Collaboration, M. Arneodo *et al.*, “A Reevaluation of the Gottfried sum,” *Phys. Rev. D* **50** (1994) R1–R3.
- [6] NuSea Collaboration, R. S. Towell *et al.*, “Improved measurement of the anti-d / anti-u asymmetry in the nucleon sea,” *Phys. Rev. D* **64** (2001) 052002, [arXiv:hep-ex/0103030](#).
- [7] SeaQuest Collaboration, J. Dove *et al.*, “The asymmetry of antimatter in the proton,” *Nature* **590** no. 7847, (2021) 561–565, [arXiv:2103.04024 \[hep-ph\]](#). [Erratum: *Nature* 604, E26 (2022)].
- [8] FNAL E906/SeaQuest Collaboration, C. H. Leung *et al.*, “Final SeaQuest Results on the Flavor Asymmetry of the Proton Light-Quark Sea with Proton-Induced Drell-Yan Process,” *Phys. Rev. Lett.* **136** no. 17, (2026) 171901, [arXiv:2512.17564 \[hep-ex\]](#).
- [9] CMS Collaboration, S. Chatrchyan *et al.*, “Measurement of the lepton charge asymmetry in inclusive W production in pp collisions at $\sqrt{s} = 7$ TeV,” *JHEP* **04** (2011) 050, [arXiv:1103.3470 \[hep-ex\]](#).

- [10] **ATLAS** Collaboration, G. Aad et al., “Measurement of W^\pm -boson differential cross-sections in proton-proton collisions with low pile-up data at $\sqrt{s} = 5.02$ TeV and 13 TeV with the ATLAS detector,” *Eur. Phys. J. C* **85** no. 7, (2025) 729, arXiv:2502.09403 [hep-ex].
- [11] **D0** Collaboration, V. M. Abazov et al., “Measurement of the electron charge asymmetry in $p\bar{p} \rightarrow W + X \rightarrow e\nu + X$ decays in $p\bar{p}$ collisions at $\sqrt{s} = 1.96$ TeV,” *Phys. Rev. D* **91** no. 3, (2015) 032007, arXiv:1412.2862 [hep-ex]. [Erratum: *Phys.Rev.D* 91, 079901 (2015)].
- [12] **CDF** Collaboration, T. A. Aaltonen et al., “Measurement of the charge asymmetry of electrons from the decays of W bosons produced in $p\bar{p}$ collisions at $\sqrt{s} = 1.96$ TeV,” *Phys. Rev. D* **104** no. 9, (2021) 092002, arXiv:2107.04678 [hep-ex].
- [13] **STAR** Collaboration, J. Adam et al., “Measurements of W and Z/γ^* cross sections and their ratios in p+p collisions at RHIC,” *Phys. Rev. D* **103** no. 1, (2021) 012001, arXiv:2011.04708 [nucl-ex].
- [14] J. Nam, “Measurements of W and Z/γ^* cross sections and their ratios in pp collisions at STAR,” 2022. <https://arxiv.org/abs/2108.01029>.
- [15] J. C. Collins, D. E. Soper, and G. F. Sterman, “Transverse Momentum Distribution in Drell-Yan Pair and W and Z Boson Production,” *Nucl. Phys. B* **250** (1985) 199–224.
- [16] C. Bierlich et al., “A comprehensive guide to the physics and usage of PYTHIA 8.3” *SciPost Phys. Codeb.* **2022** (2022) 8, arXiv:2203.11601 [hep-ph].
- [17] T.-J. Hou et al., “New CTEQ global analysis of quantum chromodynamics with high-precision data from the LHC,” *Phys. Rev. D* **103** no. 1, (2021) 014013, arXiv:1912.10053 [hep-ph].
- [18] S. Bailey, T. Cridge, L. A. Harland-Lang, A. D. Martin, and R. S. Thorne, “Parton distributions from LHC, HERA, Tevatron and fixed target data: MSHT20 PDFs,” *Eur. Phys. J. C* **81** no. 4, (2021) 341, arXiv:2012.04684 [hep-ph].
- [19] **NNPDF** Collaboration, R. D. Ball et al., “Parton distributions from high-precision collider data,” *Eur. Phys. J. C* **77** no. 10, (2017) 663, arXiv:1706.00428 [hep-ph].
- [20] **NNPDF** Collaboration, R. D. Ball et al., “The path to proton structure at 1% accuracy,” *Eur. Phys. J. C* **82** no. 5, (2022) 428, arXiv:2109.02653 [hep-ph].
- [21] **JAM** Collaboration, N. Sato, C. Andres, J. J. Ethier, and W. Melnitchouk, “Strange quark suppression from a simultaneous Monte Carlo analysis of parton distributions and fragmentation functions,” *Phys. Rev. D* **101** no. 7, (2020) 074020, arXiv:1905.03788 [hep-ph].
- [22] C. Balazs and C. P. Yuan, “Soft gluon effects on lepton pairs at hadron colliders,” *Phys. Rev. D* **56** (1997) 5558–5583, arXiv:hep-ph/9704258.
- [23] J. P. Isaacson, *ResBos2 : precision resummation for the LHC ERA*. PhD thesis, Michigan State U., Michigan State U., 2017.
- [24] J. Isaacson, Y. Fu, and C. P. Yuan, “Improving resbos for the precision needs of the LHC,” *Phys. Rev. D* **110** no. 7, (2024) 073002, arXiv:2311.09916 [hep-ph].
- [25] J. Isaacson, Y. Fu, and C. P. Yuan, “Resbos2 and the CDF W mass measurement,” *Phys. Rev. D* **110** no. 9, (2024) 094023, arXiv:2205.02788 [hep-ph].
- [26] J. M. Campbell and R. K. Ellis, “An Update on vector boson pair production at hadron colliders,” *Phys. Rev. D* **60** (1999) 113006, arXiv:hep-ph/9905386.
- [27] J. M. Campbell, R. K. Ellis, and C. Williams, “Vector Boson Pair Production at the LHC,” *JHEP* **07** (2011) 018, arXiv:1105.0020 [hep-ph].

- [28] J. Campbell and T. Neumann, “Precision Phenomenology with MCFM,” *JHEP* **12** (2019) 034, [arXiv:1909.09117 \[hep-ph\]](#).
- [29] J. Campbell, J. Huston, and F. Krauss, *The Black Book of Quantum Chromodynamics : a Primer for the LHC Era*. Oxford University Press, 2018.
- [30] P. M. Nadolsky and C. P. Yuan, “Soft parton radiation in polarized vector boson production: Theoretical issues,” *Nucl. Phys. B* **666** (2003) 3–30, [arXiv:hep-ph/0304001](#).
- [31] P. M. Nadolsky and C. P. Yuan, “Single spin asymmetries with weak bosons at RHIC,” *Nucl. Phys. B* **666** (2003) 31–55, [arXiv:hep-ph/0304002](#).
- [32] Jae Nam, PYTHIA predictions for W^+ and W^- cross sections at STAR. Private communication.
- [33] STAR Collaboration, C. E. Allgower *et al.*, “The STAR endcap electromagnetic calorimeter,” *Nucl. Instrum. Meth. A* **499** (2003) 740–750.
- [34] CTEQ Collaboration, H. L. Lai, J. Huston, S. Kuhlmann, J. Morfin, F. I. Olness, J. F. Owens, J. Pumplin, and W. K. Tung, “Global QCD analysis of parton structure of the nucleon: CTEQ5 parton distributions,” *Eur. Phys. J. C* **12** (2000) 375–392, [arXiv:hep-ph/9903282](#).
- [35] STAR Collaboration, M. Beddo *et al.*, “The STAR barrel electromagnetic calorimeter,” *Nucl. Instrum. Meth. A* **499** (2003) 725–739.
- [36] J. J. Ethier and E. R. Nocera, “Parton Distributions in Nucleons and Nuclei,” *Ann. Rev. Nucl. Part. Sci.* **70** (2020) 43–76, [arXiv:2001.07722 \[hep-ph\]](#).
- [37] T. J. Hobbs, B.-T. Wang, P. M. Nadolsky, and F. I. Olness, “Charting the coming synergy between lattice QCD and high-energy phenomenology,” *Phys. Rev. D* **100** no. 9, (2019) 094040, [arXiv:1904.00022 \[hep-ph\]](#).
- [38] M. Guzzi *et al.*, “NNLO constraints on proton PDFs from the SeaQuest and STAR experiments and other developments in the CTEQ-TEA global analysis,” *SciPost Phys. Proc.* **8** (2022) 005, [arXiv:2108.06596 \[hep-ph\]](#).
- [39] T.-J. Hou *et al.*, “Reconstruction of Monte Carlo replicas from Hessian parton distributions,” *JHEP* **03** (2017) 099, [arXiv:1607.06066 \[hep-ph\]](#).
- [40] A. Ablat *et al.*, “CT25: Progress toward next-generation PDFs for precision phenomenology at the LHC,” **12**, 2025. [arXiv:2512.19779 \[hep-ph\]](#).
- [41] A. Ablat *et al.*, “The CT25 NNLO global analysis of parton distributions in a nucleon.” A journal publication in preparation, 2026.
- [42] W. Ma, S. Yang, M. Xie, M. Liu, L. Han, and C. P. Yuan, “Flavour asymmetry of antiquarks in nucleon and nucleus,” [arXiv:2510.08941 \[hep-ex\]](#).
- [43] A. Ruzi and B.-Q. Ma, “Redetermination of proton sea distributions,” [arXiv:2605.19918 \[hep-ph\]](#).
- [44] W. T. Giele and S. Keller, “Implications of hadron collider observables on parton distribution function uncertainties,” *Phys. Rev. D* **58** (1998) 094023, [arXiv:hep-ph/9803393](#).